

Magnetic Field Independent SERF Magnetometer

Mark Dikopoltsev,^{1,2,*} Uriel Levy,¹ and Or Katz^{3,4,†}

¹*Department of Applied Physics, The Faculty of Science,
The Center for Nanoscience and Nanotechnology,
The Hebrew University of Jerusalem, Jerusalem 9190401, Israel.*

²*Rafael Ltd, 31021, Haifa, Israel.*

³*Duke Quantum Center, Duke University, Durham, NC 27701*

⁴*Department of Electrical and Computer Engineering, Duke University, Durham, NC 27708*
(Dated: September 28, 2022)

SERF magnetometers based on dense ensembles of alkali-metal spins are precision quantum sensors that hold the record of measured and projected sensitivity to magnetic fields, in the $\mu\text{G} - \text{mG}$ range. At geomagnetic fields however, these sensors quickly lose their magnetic sensitivity due to spin decoherence by random spin-exchange collisions. Here we discover that atoms with nuclear spin $I = 1/2$ can operate in the Spin-Exchange Relaxation Free (SERF) regime but for any magnitude of the magnetic field. We counter-intuitively show that frequent collisions between a dense and optically-inaccessible ($I = 1/2$) gas with another optically-accessible spin gas ($I > 1/2$) improve the fundamental magnetic sensitivity of the latter. We analyze the performance of a dual-specie potassium and atomic hydrogen magnetometer, and project a fundamental sensitivity of about $10 \text{ aT}\sqrt{\text{cm}^3/\text{Hz}}$ at geomagnetic fields for feasible experimental conditions.

Precision sensing of magnetic fields is a cardinal technique in various scientific disciplines [1–11]. Warm ensembles of alkali-metal atoms feature an unprecedented sensitivity for measuring slowly varying and constant magnetic fields [12–16]. The high sensitivity of these sensors relies on the efficient coupling of the electron spin of each alkali-metal atom to the field and the use of a macroscopic ensemble that responds in a collective manner.

At geomagnetic field, the fundamental sensitivity of magnetometers based on alkali-metal atoms reaches a lower bound around $0.6 \text{ fT}\sqrt{\text{cm}^3/\text{Hz}}$. The dependence of this limit on the atomic number density is very weak [17], because an increase in the number of spins which probe the field leads to increased decoherence by collisions [18]. Yet, At some conditions it is possible to suppress the decoherence caused by spin-exchange collisions, which are the dominant collision process in dense ensembles of alkali atoms in their electronic ground state [13, 19, 20]. Such operation corresponds to the Spin-Exchange-Relaxation Free (SERF) regime, which features an improved fundamental sensitivity by about two orders-of-magnitudes, down to $10 \text{ aT}\sqrt{\text{cm}^3/\text{Hz}}$, where the atoms response is limited by other relaxation processes [14, 21]. To date, operation in this regime at low magnetic fields holds the record of best realized magnetic sensitivity [22].

Operation in the SERF regime however poses stringent conditions on the degree of spin-polarization of the atoms [17, 23, 24], on the selectivity of the optical transitions [25], or on the magnitude of the ambient magnetic field [13–15, 26–33]. Near unity polarized spins are less susceptible to spin-exchange relaxation but typically require high optical power at pulsed operation. Opera-

tion at low magnetic fields on the other hand, requires high atomic densities, and is practically limited to a few milligauss. The low-field requirement often renders the SERF regime impractical for most applications which operate in a magnetically unshielded environment, in the presence of earth’s magnetic field (a few hundreds of milligauss).

Here we propose and analyze the operation of a hydrogen-based magnetometer which operates in the SERF regime and is unrestricted to low magnetic fields. We first discover that hydrogen atoms are inherently free of spin-exchange relaxation at any magnetic field or degree of spin-polarization, owing to their simple spin structure. We then analyze the operation of a hybrid potassium-hydrogen magnetometer, which enables control and measurement of the optically inaccessible spin-state of the hydrogen ensemble through its efficient collisional coupling. We demonstrate that the potassium atoms inherit the coherent spin properties of the hydrogen, and can therefore attain an improved fundamental sensitivity down to $10 \text{ aT}\sqrt{\text{cm}^3/\text{Hz}}$ at high magnetic fields. We finally outline an experimentally feasible configuration for realizing such a sensor.

The main limitation on the sensitivity of warm atomic magnetometers operating at high magnetic fields originates from relaxation induced by frequent spin-exchange collisions. In the mean-field (single-spin) picture [19, 34–37], collisions predominantly alter the internal spin distribution of each atom, and drive it to follow a spin-temperature distribution (STD). The ground-state energy levels of alkali-metal atoms, whose nuclear spin I is nonzero, are split into two different hyperfine manifolds with quantum numbers F, m (with $F = I \pm S$ and $|m| \leq F$) and have a density matrix $\rho(F, m) \propto e^{\beta m}$,

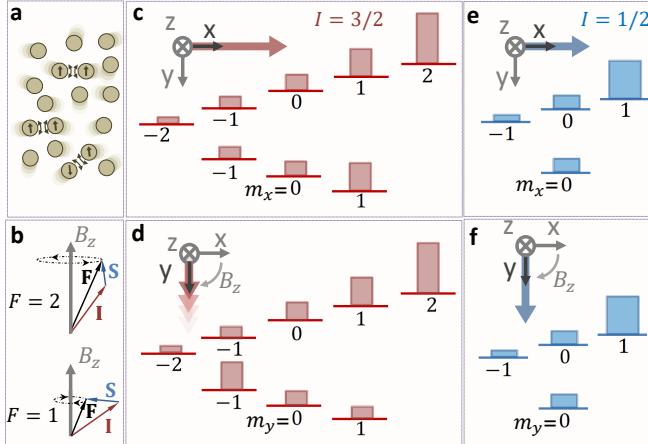


Figure 1. **Spin-exchange relaxation** **a**, Frequent binary collisions of warm atomic gas lead to efficient exchange of spin. **b**, Alkali-metal atoms with a single valence electron are comprised of two hyperfine manifolds in the electronic ground-state. The total spin \mathbf{F} precesses clockwise (counterclockwise) in the upper (lower) manifold in between sudden collisions. **c-d**, Spin-exchange relaxation mechanism for atoms with nuclear spin $I = 3/2$. **c**, For spin ensembles oriented along x , the populations of the spin levels follow a spin temperature distribution (STD) $\rho \propto e^{\beta m_x}$, the equilibrium state by collisions. **d**, Spin-precession by the magnetic field along z deters the STD, leading to decoherence by collisions; e.g. after a $\pi/2$ pulse the spin distribution is $\rho \propto e^{(-1)^F \beta m_y}$ instead, where the population in the lower hyperfine manifold is inverted. **e-f**, Precession of spin $1/2$ atoms maintains the spin-temperature distribution at all times, thus suppressing the relaxation associated with spin-exchange collisions. **c,e**, Distributions at $t = 0$ with quantization axis along \hat{x} . **d,f**, Distributions at $t = \pi/(2\gamma B_z)$ with quantization axis along \hat{y} .

following STD, as shown in Fig. 1. The inverse temperature coefficient $\beta(P)$ depends on the degree of spin-polarization of the vapor $0 \leq P \leq 1$, which is a conserved quantity in the absence of other relaxation processes [38]. For this distribution and at ambient conditions, the two hyperfine manifolds are populated independently of the hyperfine energy splitting.

A magnetic field can perturb the spin-distribution of the atoms, and compete with spin-exchange collisions which act to maintain it at STD. In the presence of a magnetic field, the spins experience Larmor precession, whose rate varies between the two hyperfine manifolds. For atoms with $I > 1/2$, the electron spin in the upper hyperfine manifold is aligned with the field, but is anti-aligned at the lower manifold. Consequently, the total spin in the two hyperfine manifolds precess at the same rate $\gamma = \gamma_e/(2I + 1)$ but at opposite directions where $\gamma_e = 28 \text{ MHz/mT}$ is the electron gyromagnetic-ratio. The opposite precession rates drive the system away from a spin-temperature distribution due to dif-

ferential rotation of the two hyperfine manifolds. For example, a spin oriented transverse to the field and initially in a spin temperature distribution $\rho \propto e^{\beta m}$, would end in a distribution of $\rho \propto e^{(-1)^F \beta m}$ after a precession time of $\pi/(2\gamma B_z)$, as illustrated in Fig. 1d. It is this deviation from STD that causes the decoherence associated with spin-exchange collisions. For spin-ensembles aligned along the field, or when the Larmor frequencies are synchronized by optical means [25], there is no precession and therefore no spin-exchange decoherence. In the SERF regime, the deviation from STD is small; either the lower hyperfine manifold is barely populated at near unity spin-polarization, or the magnetic field perturbing the STD is weaker with respect to the spin-exchange collisions rate $R \gg \gamma B$.

For atoms with $I = 1/2$ however, the lower hyperfine manifold is composed of a single level with $m = 0$ as shown in Fig. 1e-f. Consequently, a magnetic field generates precession of the magnetic moment in the upper hyperfine manifold only, and the STD is always maintained. It is therefore expected that atoms with $I = 1/2$ would be inherently in the SERF regime, regardless of the strength of the Larmor precession γB and polarization P .

We demonstrate this inherent suppression of spin-exchange relaxation for $I = 1/2$ for spins initially in a STD, using two different models. First, we solve the hyperfine Bloch equations for atoms with nuclear spin I , and describe the dynamics of the average spin of the two hyperfine manifolds in the low polarization limit [19, 25, 39]. These equations account for the magnetic field precession at a rate γB , spin exchange collisions at a rate $R = 10^6 \text{ s}^{-1}$, and taking a fixed longitudinal spin lifetime $T_1 = 10 \text{ ms}$ for all values of I . In Fig. 2(a-b) we present the decoherence rate Γ for spins oriented transverse to the field and gyromagnetic ratio γ_{eff} as a function of magnetic field. For $I > 1/2$ atoms, at high magnetic fields ($\gamma B \gg R$, practically including also geomagnetic fields, denoted by a dashed vertical line), the relaxation is dominated by spin-exchange collisions and is suppressed only at low magnetic fields. $I = 1/2$ atoms in contrast, feature a constant and reduced decoherence rate which is solely governed by their finite lifetime. The gyro-magnetic ratio for $I = 1/2$ atoms is also independent of the magnetic field, unlike all other atoms experiencing spin-exchange collisions.

To further validate the inherent SERF property of $I = 1/2$ atoms we explore an additional model. We solve the Unitary spin-exchange evolution for pairs of alkali-like spins initially in a STD. During a collision, the two valence electrons of a pair decompose into a Singlet and Triplet states, which acquire different phases, where their relative phase ϕ governs the transition amplitudes of the evolution. At room-temperature and

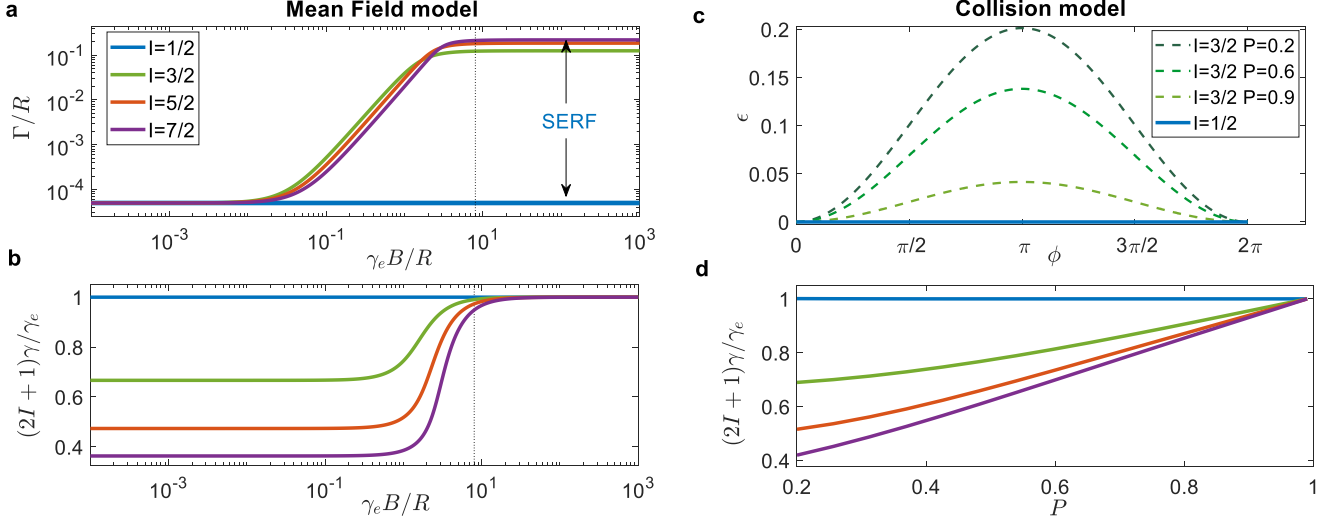


Figure 2. **Suppression of Spin-Exchange relaxation and frequency slowing-down for $I = 1/2$ atoms.** **a**, The transverse decoherence rate Γ of $I > 1/2$ atoms is dominated by spin-exchange at high magnetic field B . In contrast, the relaxation rate of $I = 1/2$ atoms (blue) is highly suppressed at all magnetic fields; it is determined by the finite lifetime but independent of the spin-exchange rate R . **b**, The gyromagnetic-ratio γ depends on magnetic field magnitude for all atoms but $I = 1/2$. **c**, Single events of spin-exchange collisions with relative scattering phase ϕ between the singlet and triplet states redistribute the magnetic coherence for all $I = 3/2$, mostly at low degrees of polarization P , but not for $I = 1/2$ (at any P). The unitless parameter ϵ quantifies the distribution of the magnetic coherence between the hyperfine manifold by collisions (See text). **d**, In the weak field limit ($\gamma_e B \ll R$), the gyromagnetic-ratio of $I > 1/2$ atoms depends on the degree of spin polarization, but is constant for $I = 1/2$ atoms. The gyromagnetic-ratio determines the slowing-down factor $q = \gamma_e/\gamma$. **a-b** are obtained from the hyperfine Bloch equations in the low polarization regime and **c-d** from a numerical stochastic model.

above, ϕ is almost uniformly distributed between 0 to 2π [21, 40–43]. The outcome of a collision for an initial two-body density matrix $\rho_a \otimes \rho_b$ is then given by [21, 44]

$$\rho = \Pi_T \rho_a \otimes \rho_b \Pi_T + e^{i\phi} \Pi_S \rho_a \otimes \rho_b \Pi_S, \quad (1)$$

where Π_S and Π_T are the projection operators on the singlet and triplet states respectively. We estimate the average amount of spin transfer between the two hyperfine states by the unitless quantity $\epsilon_+^a = (\langle F_{\text{out}}^{(+a)} \rangle - \langle F_{\text{in}}^{(+a)} \rangle) / (\langle F_{\text{in}}^{(+a)} \rangle + \langle F_{\text{in}}^{(+b)} \rangle)$ which is presented in Fig. 2c., using $\langle F_{\text{in/out}}^{(+a)} \rangle = \text{Tr}(\rho F_+^{(a)})$. For $I = 3/2$ atoms, $\epsilon_+^a > 0$ and the magnetic moments are redistributed by collisions, depending on the value of ϕ . The spin at the upper hyperfine manifold for $I = 1/2$ atoms in contrast, is unaffected for any ϕ .

We further extend our previous numerical estimations of the gyromagnetic ratio and relaxation rate for any degree of spin-polarization. We simulate the Unitary magnetic evolution of pairs of atoms in between collisions, but to keep the computational space tractable, trace out the inter-atomic coherence developed after each collision with a random ϕ by setting $\rho \rightarrow \text{Tr}_b(\rho) \otimes \text{Tr}_a(\rho)$. We characterize the gyromagnetic ratio as a function of the spin-polarization P in the low magnetic field regime and show it in Fig. 2d, where $q = \gamma_e/\gamma$ denotes the

slowing-down factor [38]. While the effective gyro magnetic ratio depends on the polarization P for all $I > 1/2$ atoms, it is independent of P for $I = 1/2$. We verify convergence and confirm the agreement of this model with the hyperfine-Bloch equations in the low polarization regime.

The hydrogen atom has a single valence electron and its nuclear spin is $I = 1/2$. It could therefore be utilized as an inherent SERF magnetometer. Its most stable form appears as a molecule H_2 , which can be efficiently dissociated via e.g., application of high-frequency RF discharge. Once dissociated, it can maintain its atomic form for long time before associating back into a molecule as this process typically requires three bodies [45–51]; 1 Torr of atomic hydrogen in a cm-size enclosure can last about a hundred of milliseconds, as traditionally utilized in precision masers [52–56].

A primary challenge in usage of atomic hydrogen relates to its energetic excited state, which hinders optical manipulation or readout of its ground state using standard laser frequencies, since its optical transitions are in the UV. Masers overcome this challenge by using non-optical methods [57–59]; pumping the hydrogen spins using permanent magnets in a Stern-Gerlach configuration, and reading their state using microwave cavities. Here we consider another approach based on a hybrid

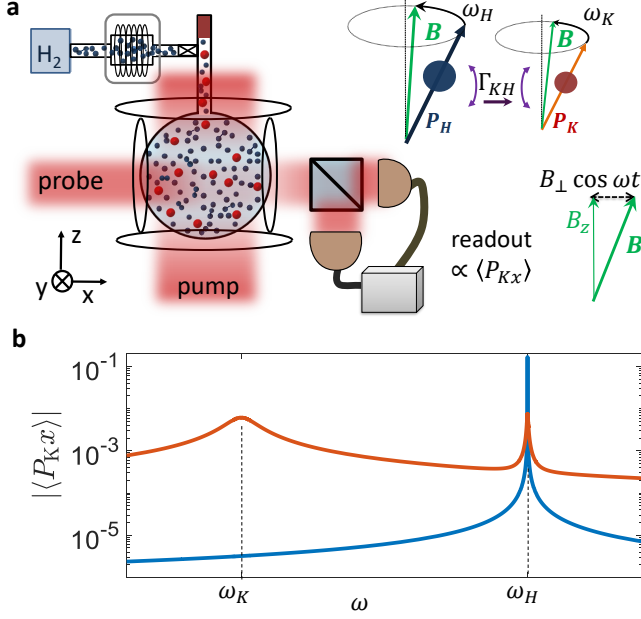


Figure 3. Operation of a dual potassium-hydrogen magnetometer. **a**, Configuration of a dual-specie magnetometer. Atomic hydrogen ($I = 1/2$) precesses around a magnetic field $B_z \hat{z}$ using a weak magnetic drive $B_\perp \cos(\omega t) \hat{x}$, and imprints its precession on a dilute potassium spin gas ($I = 3/2$). The optically-controlled potassium spins continuously polarize and read the state of the hydrogen spins. **b**, Calculated magnetic response of the potassium spins to the oscillatory magnetic drive. The potassium spins, dressed by the interaction with the hydrogen spins, feature a double resonance spectrum with resonance frequencies ω_K and $\omega_H = 2\omega_K$, as shown in red line for a low hydrogen density. At optimal conditions, the hydrogen density is higher and the imprinted hydrogen response dominates the potassium magnetic spectrum (blue line). Red and blue lines correspond to cross and star symbols in Fig. 4.

configuration where the hydrogen is collisionally coupled to another optically accessible ensemble of alkali-metal atoms [60–63].

We consider a gaseous mixture of atomic hydrogen with potassium atoms ($I = 3/2$) as illustrated in Fig. 3a. The potassium spin-polarization vector \mathbf{P}_K is optically-pumped continuously along the magnetic field $B_z \hat{z}$, and its transverse component in the xy plane can be optically probed using standard techniques [64, 65]. The potassium spins are coupled to the ensemble of hydrogen spins with mean polarization vector \mathbf{P}_H via mutual spin exchange collisions, which act to equilibrate the spin-polarization of the two ensembles.

This collisional coupling enables pumping of the hydrogen spins and also imprinting their precession on the measured response of the potassium. We can force the hydrogen precession by application of a weak and transverse magnetic field $B_\perp \cos(\omega t) \hat{x}$, whose modulation is

resonant with the hydrogen frequency $\omega_H = \gamma_H B$ but off resonant from the potassium $\omega_K = \gamma_K B = \omega_H/2$ at high magnetic fields. Including spin-relaxation of the valence electron for both species at rates R_{sd}^K, R_{sd}^H and optical pumping of the potassium electrons at rate R_p along \hat{z} , we can describe the coupled dynamics with the set of Bloch equations

$$\begin{aligned} \dot{\mathbf{P}}_H &= \gamma_H \mathbf{B} \times \mathbf{P}_H + \Gamma_{HK} \mathbf{P}_K - \Gamma_H \mathbf{P}_H + \boldsymbol{\xi}_H, \\ \dot{\mathbf{P}}_K &= \gamma_K \mathbf{B} \times \mathbf{P}_K + \Gamma_{KH} \mathbf{P}_H - \Gamma_K \mathbf{P}_K + \Gamma_p \hat{z} + \boldsymbol{\xi}_K. \end{aligned} \quad (2)$$

Here $\mathbf{B}(t) = B_z \hat{z} + B_\perp \cos(\omega t) \hat{x}$ denotes the total magnetic field vector and $\Gamma_{HK} = k_{HK} n_K / q_H$ and $\Gamma_{KH} = k_{HK} n_H / q_K$ are the hybrid spin-exchange rates, where n_K, n_H are the potassium and hydrogen number-densities, $k_{HK} = 5.4 \times 10^{-10} \text{ cm}^3/\text{s}$ is the mutual spin-exchange rate coefficient [61] and q_H and q_K are the slowing-down factors of the two species [38] presented in Fig. 2d. We take $\Gamma_p = R_p / q_K$ as the optical pumping rate and $\Gamma_K = \Gamma_p + \Gamma_{KH} + (R_{sd}^K + R_{se}^K) / q_K$ and $\Gamma_H = \Gamma_{HK} + R_{sd}^H / q_H$ as the transverse relaxation rates of the two ensembles. The hydrogen spins relax by spin-destruction processes or spin-exchange collisions with the potassium spins, but crucially, are free of spin-exchange relaxation by rapid collisions with other hydrogen atoms (i.e., $R_{se}^H = 0$).

We introduce the white noise vector processes $\boldsymbol{\xi}_H$ and $\boldsymbol{\xi}_K$ transverse to the polarization axis to describe the Atom Projection Noise (APN) that limits the fundamental sensitivity of the magnetometer (i.e. the standard quantum limit) [32, 66]. They satisfy $\langle \boldsymbol{\xi}_H(t) \rangle = \langle \boldsymbol{\xi}_A(T) \rangle = 0$ but have a nonzero variance $\langle \xi_{qi}(t) \xi_{q'j}(t') \rangle = \delta_{ij} \delta_{qq'} \delta(t-t') R_q / (n_q V)$ for $q, q' \in \{K, H\}$ and $i, j \in \{x, y\}$.

We begin by presenting an approximate analytical solution of Eqs. (2) to illustrate the coupled dynamics, and then present more general numerical results. We consider the regime in which the Hydrogen is the dominant specie $n_H \gg n_K$ and assume the rotating wave approximation such that $\omega \gtrsim \Gamma_K, \Gamma_{KH} \gg \Gamma_H$. By continuous optical pumping the potassium spins reach a steady polarization of

$$P_{Kz} = \frac{\Gamma_p \Gamma_H}{\Gamma_K \Gamma_H - \Gamma_{KH} \Gamma_{HK}}. \quad (3)$$

Sizeable polarization requires pumping rate that scales as $\Gamma_p \sim n_H k_{HK}$, accounting for the transfer of spin polarization from the rare potassium vapor to the dense hydrogen gas. In the presence of the weak driving field $\gamma_H B_\perp \lesssim \Gamma_H$, the mean response of the transverse potassium spin $\langle P_{K+} \rangle = \langle P_{Kx} + iP_{Ky} \rangle$ at the drive frequency ω is dominated by the coupling to the driven hydrogen and in the rotating frame is given by

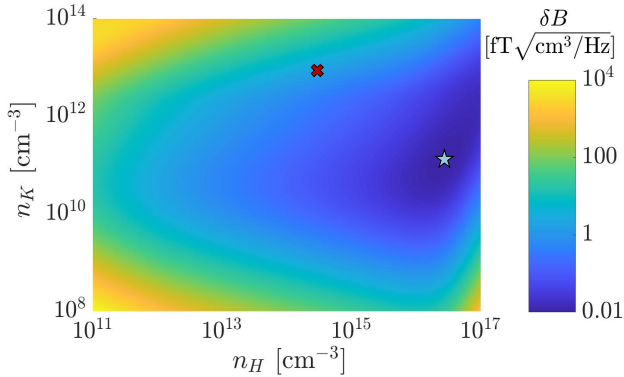


Figure 4. **Projected Fundamental sensitivity.** The magnetic sensitivity of the hydrogen-potassium magnetometer limited by atom-projection noise, and independent of the magnetic field magnitude. Cross and star correspond to the configurations presented in Fig. 3b in red and blue lines respectively.

$$\langle P_{K+}(\omega) \rangle = \frac{i\gamma_K B_{\perp} P_{Kz}}{\Gamma_H \left(1 - \frac{(\Gamma_K - i(\omega_K - \omega))}{\Gamma_{KH}} \frac{(\Gamma_H - i(\omega_H - \omega))}{\Gamma_{HK}}\right)}. \quad (4)$$

The spectral response of Eq. (4) has a double resonance shape, a broad complex Lorentzian centered at ω_K with linewidth Γ_K , and a narrow complex Lorentzian centered at ω_H and linewidth Γ_H , as shown in Fig. 3b (red line). The former corresponds to the response of the potassium to oscillations at its bare resonance, which is broadened by rapid collisions with the hydrogen and optical pumping. The latter and stronger resonance, manifests the efficient response of hydrogen atoms to the field, imprinted on the potassium response by rapid spin-exchange collisions.

The narrow resonance line at $\omega = \omega_H$ is associated with a sharp variation of the phase of $\langle P_{K+} \rangle$ which in turn allows for sensitive estimation of the resonance frequency ω_H and therefore of the magnetic field B_z . We estimate the magnetic sensitivity in this configuration due to APN by linearizing the response of Eq. (4) around $\omega - \omega_H$ and computing the APN variance, see Appendix A. To reveal the qualitative scaling of the magnetic noise, we assume the simplifying conditions $\Gamma_H \sim \Gamma_{HK}$ and $\Gamma_K \sim \Gamma_{KH}$ and find that for a measurement volume V , the spin variance of the potassium scales as $\langle |\Delta P_{K+}(\omega = \omega_H)|^2 \rangle \propto t/(\Gamma_H n_H V)$, and the fundamental magnetic sensitivity is limited by the effective magnetic noise

$$\delta B_{\text{APN}} \propto \frac{1}{\gamma_H} \sqrt{\frac{\Gamma_H}{n_H V}}. \quad (5)$$

Remarkably, the fundamental sensitivity in this configuration is determined by the Hydrogen properties: its

high number-density and its narrow linewidth, therefore enabling high sensitivity at large magnetic fields $\gamma_H B \gg \Gamma_H$. Comparison of this response to a single-specie potassium magnetometer, whose low density is tuned to set $\Gamma_K = \Gamma_H$, reveals that the sensitivity in the proposed hybrid configuration is enhanced by a large factor that scales as $\sqrt{n_H/n_K}$.

To quantitatively analyze the magnetometer performance, we numerically calculate the fundamental sensitivity as a function of n_K and n_H , and at each point optimize for the optical pumping rate Γ_p and the amplitude of the magnetic drive B_{\perp} . We take $\Gamma_H = 40 \text{ s}^{-1}$ and present the calculated fundamental sensitivity in Fig. 4. We find a fundamental magnetic sensitivity of $\delta B_{\text{APN}} = 10 \text{ aT} \sqrt{\text{cm}^3/\text{Hz}}$ as marked by a cyan star for $n_K = 1.2 \times 10^{11} \text{ cm}^{-3}$, $n_H = 2.7 \times 10^{16} \text{ cm}^{-3}$ using $B_{\perp} = 0.35 \text{ nT}$ and $\Gamma_p = 1.2 \times 10^7 \text{ s}^{-1}$, which correspond to about 1.5 W of pump beam power in a 1" diameter cell. The spectral response of the potassium at these conditions is plotted in Fig. 3 with a blue line and the configuration associated with the red line is marked with a red cross in Fig. 4.

In summary, we proposed and analyzed using the mixture of hydrogen-potassium atoms for a precision optical magnetometer. Owing to their simple spin structure, hydrogen atoms ($I = 1/2$) are free of spin-exchange relaxation at any magnetic field and spin-polarization, enabling the potential operation of this magnetometer in the ultra-sensitive SERF regime at geomagnetic fields.

It is interesting to compare the operation of this hybrid magnetometer with other precision dual species sensors such as alkali-metal and noble gas comagnetometers [2, 64, 67, 68]. In comagnetometers, the alkali spin is utilized for pumping and probing of noble-gas spins, which are used for precision sensing of external fields. The coupling between noble-gas atoms to alkali-metal spins relies on the weak Fermi-contact interaction, and can attain high sensitivity which is limited to an ultranarrow bandwidth set by their long lifetime [1, 6, 69]. Our configuration in contrast, relies on strong exchange interaction between the valence electrons of the two species, and the efficient response of the hydrogen atoms to magnetic fields.

Furthermore, the hybrid hydrogen-potassium configuration is potentially more accurate with respect to other single-specie SERF magnetometers; The hydrogen's gyromagnetic ratio is known to a high accuracy, and unlike atoms with $I > 1/2$, it is independent of the degree of spin polarization or magnitude of the magnetic field.

Finally, it is intriguing to consider the operation of this configuration from a spin-noise perspective. The spin noise of dual specie configurations has been analyzed theoretically and experimentally in [66], demonstrating that spin-exchange coupling with another

specie acts to increase the measured noise variance. Here we also find that the potassium spin-projection noise is increased by a factor $\sim \sqrt{n_H/n_K}$. It is the improvement of the potassium signal by a larger factor $\sim n_H/n_K$ that leads to the enhanced sensitivity of this hybrid sensor. The dressed hydrogen-potassium state can potentially also be implemented in other emerging avenues such as in efficient generation of spin-entanglement [28, 70–73] and other quantum optics applications [74–77].

* mark.dikopoltsev@mail.huji.ac.il

† or.katz@duke.edu

- [1] M. Jiang, H. Su, A. Garcon, X. Peng, and D. Budker, Search for axion-like dark matter with spin-based amplifiers, *Nature Physics* **17**, 1402 (2021).
- [2] T. R. Gentile, P. Nacher, B. Saam, and T. Walker, Optically polarized he 3, *Reviews of modern physics* **89**, 045004 (2017).
- [3] K. Jensen, R. Budvytyte, R. A. Thomas, T. Wang, A. M. Fuchs, M. V. Balabas, G. Vasilakis, L. D. Mosgaard, H. C. Staerkind, J. H. Müller, *et al.*, Non-invasive detection of animal nerve impulses with an atomic magnetometer operating near quantum limited sensitivity, *Scientific reports* **6**, 1 (2016).
- [4] J. Hernandez, G. Cifuentes-Nava, E. Cabral-Cano, I. Hrvoic, F. Lopez, and M. Wilson, Ultrasensitive geomagnetic field temporal variations and its relationship to stress in the earth’s crust: an experiment in the oaxaca coast, mexico., in *AGU Spring Meeting Abstracts*, Vol. 2007 (2007) pp. GP21A–03.
- [5] G. Oelsner, R. IJsselsteijn, T. Scholtes, A. Krüger, V. Schultze, G. Seyffert, G. Werner, M. Jäger, A. Chwala, and R. Stolz, Integrated optically pumped magnetometer for measurements within earth’s magnetic field, *Physical Review Applied* **17**, 024034 (2022).
- [6] I. M. Bloch, G. Ronen, R. Shaham, O. Katz, T. Volansky, and O. Katz, New constraints on axion-like dark matter using a floquet quantum detector, *Science advances* **8**, eabl8919 (2022).
- [7] L. Neukirch, T. Kornack, and J. Tarduno, Development of a serf atomic magnetometer for paleomagnetic applications, in *AGU Fall Meeting Abstracts*, Vol. 2010 (2010) pp. GP11A–0756.
- [8] J. T. Robinson, E. Pohlmeier, M. C. Gather, C. Kemere, J. E. Kitching, G. G. Malliaras, A. Marblestone, K. L. Shepard, T. Stieglitz, and C. Xie, Developing next-generation brain sensing technologies-a review, *IEEE sensors journal* **19**, 10163 (2019).
- [9] S. Xu, V. V. Yashchuk, M. H. Donaldson, S. M. Rochester, D. Budker, and A. Pines, Magnetic resonance imaging with an optical atomic magnetometer, *Proceedings of the National Academy of Sciences* **103**, 12668 (2006).
- [10] M. Ledbetter, I. Savukov, D. Budker, V. Shah, S. Knappe, J. Kitching, D. Michalak, S. Xu, and A. Pines, Zero-field remote detection of nmr with a microfabricated atomic magnetometer, *Proceedings of the National Academy of Sciences* **105**, 2286 (2008).
- [11] S. Afach, B. C. Buchler, D. Budker, C. Dailey, A. Derevianko, V. Dumont, N. L. Figueroa, I. Gerhardt, Z. D. Grujić, H. Guo, *et al.*, Search for topological defect dark matter with a global network of optical magnetometers, *Nature Physics* **17**, 1396 (2021).
- [12] D. Budker and M. Romalis, Optical magnetometry, *Nature physics* **3**, 227 (2007).
- [13] I. Kominis, T. Kornack, J. Allred, and M. V. Romalis, A subfemtotesla multichannel atomic magnetometer, *Nature* **422**, 596 (2003).
- [14] H. Dang, A. C. Maloof, and M. V. Romalis, Ultrahigh sensitivity magnetic field and magnetization measurements with an atomic magnetometer, *Applied Physics Letters* **97**, 151110 (2010).
- [15] M. Ledbetter, I. Savukov, V. Acosta, D. Budker, and M. Romalis, Spin-exchange-relaxation-free magnetometry with cs vapor, *Physical Review A* **77**, 033408 (2008).
- [16] R. Gartman, V. Guarrera, G. Bevilacqua, and W. Chalupczak, Linear and nonlinear coherent coupling in a bell-bloom magnetometer, *Physical Review A* **98**, 061401 (2018).
- [17] S. Smullin, I. Savukov, G. Vasilakis, R. Ghosh, and M. Romalis, Low-noise high-density alkali-metal scalar magnetometer, *Physical Review A* **80**, 033420 (2009).
- [18] W. Happer and H. Tang, Spin-exchange shift and narrowing of magnetic resonance lines in optically pumped alkali vapors, *Physical Review Letters* **31**, 273 (1973).
- [19] W. Happer and A. Tam, Effect of rapid spin exchange on the magnetic-resonance spectrum of alkali vapors, *Physical Review A* **16**, 1877 (1977).
- [20] A. Korver, R. Wyllie, B. Lancor, and T. Walker, Suppression of spin-exchange relaxation using pulsed parametric resonance, *Physical review letters* **111**, 043002 (2013).
- [21] Y.-Y. Jau, T. Walker, and W. Happer, *Optically pumped atoms* (John Wiley & Sons, 2010).
- [22] J. Allred, R. Lyman, T. Kornack, and M. V. Romalis, High-sensitivity atomic magnetometer unaffected by spin-exchange relaxation, *Physical review letters* **89**, 130801 (2002).
- [23] Y.-Y. Jau, A. Post, N. Kuzma, A. Braun, M. Romalis, and W. Happer, Intense, narrow atomic-clock resonances, *Physical review letters* **92**, 110801 (2004).
- [24] D. Sheng, S. Li, N. Dural, and M. V. Romalis, Subfemtotesla scalar atomic magnetometry using multipass cells, *Physical review letters* **110**, 160802 (2013).
- [25] A. Berrebi, M. Dikopoltsev, O. Katz, and O. Katz, Optical protection of alkali-metal atoms from spin relaxation, *arXiv preprint arXiv:2209.12360* (2022).
- [26] M. Balabas, T. Karaulanov, M. Ledbetter, and D. Budker, Polarized alkali-metal vapor with minute-long transverse spin-relaxation time, *Physical review letters* **105**, 070801 (2010).
- [27] W. Chalupczak, P. Josephs-Franks, B. Patton, and S. Pustelny, Spin-exchange narrowing of the atomic ground-state resonances, *Physical Review A* **90**, 042509 (2014).
- [28] J. Kong, R. Jiménez-Martínez, C. Troullinou, V. G. Lucivero, G. Tóth, and M. W. Mitchell, Measurement-induced, spatially-extended entanglement in a hot,

- strongly-interacting atomic system, *Nature communications* **11**, 1 (2020).
- [29] R. Jimenez-Martinez, S. Knappe, and J. Kitching, An optically modulated zero-field atomic magnetometer with suppressed spin-exchange broadening, *Review of Scientific Instruments* **85**, 045124 (2014).
- [30] O. Katz, M. Dikopoltsev, O. Peleg, M. Shuker, J. Steinhauer, and N. Katz, Nonlinear elimination of spin-exchange relaxation of high magnetic moments, *Physical review letters* **110**, 263004 (2013).
- [31] W. Xiao, T. Wu, X. Peng, and H. Guo, Atomic spin-exchange collisions in magnetic fields, *Physical Review A* **103**, 043116 (2021).
- [32] K. Mouloudakis, G. Vasilakis, V. Lucivero, J. Kong, I. Kominis, and M. Mitchell, Effects of spin-exchange collisions on the fluctuation spectra of hot alkali vapors, *arXiv preprint arXiv:2204.08748* (2022).
- [33] M. Dikopoltsev, A. Berrebi, U. Levy, and O. Katz, Suppressing the decoherence of alkali-metal spins at low magnetic fields, *arXiv preprint arXiv:2209.12236* (2022).
- [34] L. W. Anderson, F. M. Pipkin, and J. C. Baird Jr, N 14-n 15 hyperfine anomaly, *Physical Review* **116**, 87 (1959).
- [35] W. Happer, Optical pumping, *Reviews of Modern Physics* **44**, 169 (1972).
- [36] I. Savukov and M. Romalis, Effects of spin-exchange collisions in a high-density alkali-metal vapor in low magnetic fields, *Physical Review A* **71**, 023405 (2005).
- [37] Y. Horowicz, O. Katz, O. Raz, and O. Firstenberg, Critical dynamics and phase transition of a strongly interacting warm spin gas, *Proceedings of the National Academy of Sciences* **118**, e2106400118 (2021).
- [38] S. Appelt, A. B.-A. Baranga, C. Erickson, M. Romalis, A. Young, and W. Happer, Theory of spin-exchange optical pumping of 3 he and 129 xe, *Physical review A* **58**, 1412 (1998).
- [39] O. Katz, O. Peleg, and O. Firstenberg, Coherent coupling of alkali atoms by random collisions, *Physical Review Letters* **115**, 113003 (2015).
- [40] D. E. Pritchard and F. Y. Chu, Alkali-alkali differential spin-exchange scattering. ii, *Physical Review A* **2**, 1932 (1970).
- [41] J. P. Burke, J. L. Bohn, B. Esry, and C. H. Greene, Impact of the rb 87 singlet scattering length on suppressing inelastic collisions, *Physical Review A* **55**, R2511 (1997).
- [42] D. E. Pritchard, D. C. Burnham, and D. Kleppner, Atomic differential spin-exchange scattering, *Physical Review Letters* **19**, 1363 (1967).
- [43] V. Kartoshkin, Complex cross sections of spin exchange in collisions of sodium and potassium atoms in the ground state, *Optics and Spectroscopy* **109**, 674 (2010).
- [44] O. Katz and O. Firstenberg, Synchronization of strongly interacting alkali-metal spins, *Physical Review A* **98**, 012712 (2018).
- [45] J. Slevin and W. Stirling, Radio frequency atomic hydrogen beam source, *Review of Scientific Instruments* **52**, 1780 (1981).
- [46] S. Longo and I. Boyd, Nonequilibrium dissociation of hydrogen in a parallel-plate radio frequency discharge, *Chemical physics* **238**, 445 (1998).
- [47] J. Xiao, P. Bénard, and R. Chahine, Charge-discharge cycle thermodynamics for compression hydrogen storage system, *International Journal of Hydrogen Energy* **41**, 5531 (2016).
- [48] C. Goodyear and A. Von Engel, Dissociation and ionization of hydrogen in high frequency discharges, *Proceedings of the Physical Society (1958-1967)* **79**, 732 (1962).
- [49] A. T. Bell, A model for the dissociation of hydrogen in an electric discharge, *Industrial & Engineering Chemistry Fundamentals* **11**, 209 (1972).
- [50] A. D. MacDonald and S. C. Brown, High frequency gas discharge breakdown in hydrogen, *Physical Review* **76**, 1634 (1949).
- [51] D. J. Rose and S. C. Brown, High-frequency gas discharge plasma in hydrogen, *Physical Review* **98**, 310 (1955).
- [52] G. Busca, L. Bernier, H. Schweda, N. Kardashev, V. Andreianov, I. Roxburgh, and S. Polnarev, The cronos hydrogen maser clock redshift experiment on radioastron, *Advances in Space Research* **32**, 1421 (2003).
- [53] W.-q. Zhang, C.-f. Lin, S.-l. Yu, G.-z. Wang, Y.-p. Zhang, P.-h. Yang, and J. Zhang, A study and performance evaluation of hydrogen maser user in chinese mobile vlbi stations, *Chinese Astronomy and Astrophysics* **25**, 390 (2001).
- [54] D. Kleppner, H. Berg, S. Crampton, N. Ramsey, R. F. Vessot, H. Peters, and J. Vanier, Hydrogen-maser principles and techniques, *Physical Review* **138**, A972 (1965).
- [55] H. M. Goldenberg, D. Kleppner, and N. F. Ramsey, Atomic hydrogen maser, *Physical Review Letters* **5**, 361 (1960).
- [56] H. Peters, B. Owings, T. Oakley, and L. Beno, Hydrogen masers for radio astronomy, in *Proceedings of the 41st Annual Frequency Symposium 1987* (1987) pp. 75–81.
- [57] G. A. Ruff and T. R. Carver, Spin-exchange light modulation by atomic hydrogen, *Physical Review Letters* **15**, 282 (1965).
- [58] R. L. Walsworth, I. F. Silvera, E. M. Mattison, and R. F. Vessot, Measurement of a hyperfine-induced spin-exchange frequency shift in atomic hydrogen, *Physical Review A* **46**, 2495 (1992).
- [59] M. A. Humphrey, D. F. Phillips, E. M. Mattison, R. F. Vessot, R. E. Stoner, and R. L. Walsworth, Testing cpt and lorentz symmetry with hydrogen masers, *Physical Review A* **68**, 063807 (2003).
- [60] M. Poelker, K. Coulter, R. Holt, C. Jones, R. Kowalczyk, L. Young, B. Zeidman, and D. Toporkov, High-density production of spin-polarized atomic hydrogen and deuterium, *Physical Review A* **50**, 2450 (1994).
- [61] H. Cole and R. Olson, Spin-exchange cross sections for hydrogen-atom-alkali-metal-atom collisions, *Physical Review A* **31**, 2137 (1985).
- [62] S. G. Redsun, R. Knize, G. Cates, and W. Happer, Production of highly spin-polarized atomic hydrogen and deuterium by spin-exchange optical pumping, *Physical Review A* **42**, 1293 (1990).
- [63] L. Anderson and T. Walker, Spin exchange optical pumping of hydrogen and deuterium nuclei, *Nuclear Instruments and Methods in Physics Research Section A: Accelerators, Spectrometers, Detectors and Associated Equipment* **357**, 220 (1995).
- [64] O. Katz, R. Shaham, and O. Firstenberg, Coupling light

- to a nuclear spin gas with a two-photon linewidth of five millihertz, *Science advances* **7**, eabe9164 (2021).
- [65] C. Mazzinghi, D. B. Orenes, P. Gomez, V. G. Lucivero, E. Aybar, S. Gugnani, and M. W. Mitchell, Cavity-enhanced polarization rotation measurements for low-disturbance probing of atoms, *Optics Express* **29**, 40854 (2021).
- [66] A. Dellis, M. Loulakis, and I. Kominis, Spin-noise correlations and spin-noise exchange driven by low-field spin-exchange collisions, *Physical Review A* **90**, 032705 (2014).
- [67] G. Vasilakis, J. Brown, T. Kornack, and M. Romalis, Limits on new long range nuclear spin-dependent forces set with a k- he 3 comagnetometer, *Physical review letters* **103**, 261801 (2009).
- [68] R. Shaham, O. Katz, and O. Firstenberg, Strong coupling of alkali-metal spins to noble-gas spins with an hour-long coherence time, *Nature Physics* **18**, 506 (2022).
- [69] I. M. Bloch, Y. Hochberg, E. Kuflik, and T. Volansky, Axion-like relics: new constraints from old comagnetometer data, *Journal of High Energy Physics* **2020**, 1 (2020).
- [70] K. Mouloudakis and I. Kominis, Spin-exchange collisions in hot vapors creating and sustaining bipartite entanglement, *Physical Review A* **103**, L010401 (2021).
- [71] V. Guarrera, R. Gartman, G. Bevilacqua, and W. Chalupczak, Spin-noise spectroscopy of a noise-squeezed atomic state, *Physical Review Research* **3**, L032015 (2021).
- [72] I. Kominis, Sub-shot-noise magnetometry with a correlated spin-relaxation dominated alkali-metal vapor, *Physical review letters* **100**, 073002 (2008).
- [73] H. Bao, J. Duan, S. Jin, X. Lu, P. Li, W. Qu, M. Wang, I. Novikova, E. E. Mikhailov, K.-F. Zhao, K. Mølmer, H. Shen, and Y. Xiao, Spin squeezing of 1011 atoms by prediction and retrodiction measurements, *Nature* **581**, 159 (2020).
- [74] K. Hammerer, A. S. Sørensen, and E. S. Polzik, Quantum interface between light and atomic ensembles, *Reviews of Modern Physics* **82**, 1041 (2010).
- [75] O. Katz, R. Shaham, E. S. Polzik, and O. Firstenberg, Long-lived entanglement generation of nuclear spins using coherent light, *Physical Review Letters* **124**, 043602 (2020).
- [76] A. Serafin, M. Fadel, P. Treutlein, and A. Sinatra, Nuclear spin squeezing in helium-3 by continuous quantum nondemolition measurement, *Physical Review Letters* **127**, 013601 (2021).
- [77] B. Julsgaard, J. Sherson, J. I. Cirac, J. Fiurášek, and E. S. Polzik, Experimental demonstration of quantum memory for light, *Nature* **432**, 482 (2004).